The role of the wind-transported dust in slope streaks activity: Evidence from the HRSC data

D. Baratoux

Observatoire Midi-Pyrénées, Laboratoire Dynamique Terrestre et Planétaire, UMR 5562, Toulouse, France.

N. Mangold

Interaction et Dynamique des Environnements de Surface, UMR8148, Orsay, France

F. Forget

Laboratoire de Météorologie Dynamique, Université de Paris 6, UMR 8539, Paris, France.

A. Cord

European Space Research and Technology Centre (ESTEC), European Space Agency, division SCI-SB, Noordwijk, Netherlands

P. Pinet

Observatoire Midi-Pyrénées, Laboratoire Dynamique Terrestre et Planétaire, UMR 5562, Toulouse, France

Y. Daydou

Observatoire Midi-Pyrénées, Laboratoire Dynamique Terrestre et Planétaire,

UMR 5562, Toulouse, France

A. Jehl

Observatoire Midi-Pyrénées, Laboratoire Dynamique Terrestre et Planétaire,

UMR 5562, Toulouse, France

P. Masson

Interaction et Dynamique des Environnements de Surface, UMR8148, Orsay,

France

G. Neukum

Institut für Geologische Wissenschaften, Freie Universität, Berlin, Germany

The HRSC CO-Investigator Team

Corresponding author

David Baratoux

Observatoire Midi-Pyrénées

Laboratoire Dynamique Terrestre et Planétaire

31 400 Toulouse

Tel: 33 5 61 33 29 20

Fax: 33 5 61 33 29 00

e-mail: baratoux@dtp.obs-mip.fr

D. Baratoux, Observatoire Midi-Pyrénées, Laboratoire Dynamique Terrestre et Planétaire, UMR 5562, 14 Avenue Edouard Belin, F-31400 Toulouse, France (baratoux@dtp.obs-mip.fr)

Abstract. Slope streaks are gravity-driven albedo features observed on Martian slopes since the Viking missions. The debated mechanism of formation could involve alternatively dry granular flow or wet mass wasting. A systematic mapping of slope streaks from the High Resolution Stereo Camera is presented in this paper. Two regions known for their slope streaks activity have been studied, the first one is located close to Cerberus lava flow, and the second one is inside the Olympus Mons Aureole. The statistics of slope streaks shapes measured from orthorectified images confirm previous results from Mars Orbiter Camera surveys. Preferential orientations of slope streaks are reported. Slope streaks occur preferentially on west facing slopes at latitudes lower than 30^oN for Olympus and on south-west facing slopes for Cerberus. Wind directions derived from a General Circulation Model during the dusty season correlate with these orientations. Furthermore, west facing slopes at Olympus have a thicker dust cover. These observations indicate that slope streaks are dust avalanches controlled by the preferential accumulation of dust in the downstream side of the wind flow. The paucity of slope streaks at high latitudes and their preferential orientation on south-facing slopes have been presented as an evidence for a potential role of H_2O phase transition in triggering or flow. The potential role of H_2O can not be ruled out from our observations but the dust avalanche model together with the atmospheric circulation could potentially explain all observations. The role of H_2O might be limited to a stabilizing effect of dust deposits on northward facing slopes at intermediate latitudes (30^oN-33^oN) and on all slopes further north.

keywords: Mars, surface; Geological processes

1. Introduction

Slope streaks are gravity-driven albedo features observed on Martian slopes since the Viking missions [*Ferguson and Lucchitta,* 1984]. They have been studied in details with the Mars Orbiter Camera [*Sullivan et al.,* 2001]. But a definitive explanation of these features has not been reached despite the recent efforts of global scale survey with MOC (Mars Orbiter Camera) data [*Sullivan et. al.,* 2001 ; *Schorghofer et. al.,* 2002 ; *Aharonson et al.,* 2003]. The various mechanisms which have been proposed throughout the last decades, involving alternatively dry granular flow or wet mass wasting, are still debated [*Morris,* 1982; *Sullivan et al.,* 2001; *Ferris et al.,* 2002; *Motazedian,* 2003; *Myamoto et al.,* 2004]. We identify five key questions concerning the current state of understanding of these albedo features. (1) What are the triggering mechanism and the nature of the source point? (2) What is the mechanism of emplacement until the flow comes to rest and what is the velocity, the duration of the event? (3) What is the relative contribution of the variations in composition and physical properties of the streaks to the observed contrast relatively to the adjacent terrains? (4) How can we interpret the slope streaks distribution at the global scale and the possible local associations with some geological units? (5) What is the present activity, the rate of formation and fading, and are the formation and fading rate in balance? The new data presented in this paper result from a systematic mapping of slope streaks from the HRSC instrument onboard Mars Express. The interpretation of these new observations demonstrates the role of wind in the formation of slope streaks. New insights from this systematic mapping in addressing the key questions mentioned above are also presented.

2. Slope streaks characteristics, associations and activity

2.1. Shapes

The shapes of the slope streaks have been largely described by *Sullivan et al.* [2001] from the analysis of numerous MOC images. The slope streaks are fan-shaped with sharp boundaries, the limits of these albedo features are never diffuse. No indication of relief associated to these features has been found [*Gerstell et al.,* 2005]. Typical lengths of these streaks range from 300 to 500 meters, slope streaks longer than 2 km are considered unusual. The widths of these objects are generally below 200 meters. The ratio length/width is highly variable and ranges from 5 to 30. Digitation is frequent at the edge of the deposit and appears sometimes at mid-slope. The source point of the slope streak is never resolved at the MOC resolution and is consequently smaller than 2-3 meters. Sometimes, a distinct boulder or a topographic perturbation is seen at the apex of the streak.

2.2. Contrast and photometric properties

Slope streaks can be darker or brighter in comparison with their surrounding, but dark streaks are far more common than bright ones. We emphasize here that the contrast is usually weak, up to 10% for the dark slope streaks and only up to 2% for the bright slope streaks [*Sullivan et al.,* 2001]. The apparent strong contrast is due to the stretch of the MOC images of dusty regions for which the albedo variations are generally low. There is no strong or systematic variations in albedo along the slope within the feature. However, few examples can be found where the contrast on the surrounding terrain reverses. In this case, the source area is the brighter one. A photometric effect, for instance a change in the surface roughness or sizes of particles, could be invoked to explain the occurrence of bright and dark slope streaks. A dependence of the apparent contrast with the conditions

of illumination is expected as suggested by some examples (e.g., Fig. 1) but bright and dark slope streaks are often intermingled on the same slopes (e.g., Fig. 2). *Sullivan et al.* [2001] mentioned this second observation to rule out the photometric effect. However, ruling out the photometric hypothesis from this observation implicitly assumes that, if photometric parameters were modified along the streaks, they would be always modified in the same manner, for instance an increase of the mean size of the particle. This is not demonstrated, and the processes forming the streaks could modify photometric parameters in various ways, resulting in both darker and brighter surfaces. It is thought here that the presence of bright and dark slope streaks still raises the question of the contribution of the physical surface state to the observed contrast. The stronger contrast for dark slope streaks (up to 10%) than for bright slope streaks (2%) relatively to the adjacent terrains requires a satisfactory explanation. Furthermore, the bright slopes streaks have been observed in Amazonis Planitia and Arabia Terra but were not recorded in Tharsis by *Sullivan et al.* [2001], a region where slope streaks are common. Bright slope streaks are now known to occur in Tharsis as well (see for instance, MOC image M2000342), but could be less common.

2.3. Dynamic properties

Slope streaks seems to be strongly influenced by the local slope gradient suggesting a low inertia. However, when two slope streaks intersect, it seems that one slope streak forms an obstacle for the flow or limits the supply of granular material stopping the propagation of the flow (MOC image M03-07769 located on the Olympus Aureole; see *Sullivan et al.* [2001]). The dynamic properties of slope streaks could result from the destabilization of granular material. The dynamics of granular material is controlled by the critical angle

at which the avalanche is triggered, and the angle of repose at which the material comes at rest. Sources of slope streaks can be found both at mid-slope or on apparently steeper crests. This observation implies that the ranges of slope angles where slope streaks occur greatly exceeds what could be expected for a phenomenon of destabilization of granular material composed of large particles like sands [*Sullivan et al.,* 2001].

2.4. Distribution and associations

At the local scale, some slope streaks seem to be associated with crater rim interiors, caldera walls, trough walls and knobs. In some places, they seem to originate from the same stratigraphic unit, but this is far from systematic, and it is not possible to identify unambiguously the outcrop from where the material originates. At the scale of the planet, slope streaks are not associated with a terrain of particular age. They can be found both on relatively old units (Arabia Terra, Noachian) and very recent units (Olympus lavas, Elysium area, Late Amazonian). Slope streaks occur where the RMS surface slope as defined by *Schorghofer et al.* [2002] is greater than 0.9^o. The presence of slopes is an obvious condition for gravity-driven processes. Slope streaks are always associated with low thermal inertia (in general below 150 $Jm^{-2}s^{1/2}K^{-1}$) and high albedo regions. This association strongly suggests the presence of dusty material (particles of a few microns in size) on the slopes as a necessary condition for slope streaks formation. *Schorghofer et al.* [2002] demonstrated that slope streaks occur only in places where the Martian temperature as measured by TES exceeds at least once a Martian year 275 K, a value remarkably close to the triple point of water. This observation suggests that small amounts of H_2O are present in low-latitude near-surface regions and undergo phase transition (melting or

sublimation) at time of high insolation. Such a phase transition could play a role in the triggering or fluidization of the slope streaks.

2.5. Activity and evolution

Slope streaks formation is known to be an active process since the Mars Global Surveyor mission. The MOC instrument revealed that slope streaks are currently forming on the surface of Mars [*Malin and Edgett,* 2001]. Using 181 overlapping MOC image pairs containing 2500 streaks, *Aharonson et al.* [2003] found 126 new slope streaks. They estimate a formation rate, defined as the number of new streaks per year relative to the number of streaks in the overlapping area :

$$q = \frac{\Delta n}{n \Delta t} \tag{1}$$

where n is the number of slope streaks in the overlap region, Δn the number of new slope streaks and Δt is the time interval between the two images. Rates of formation at the regional scale have been found to be on average 7% per existing streak per Martian year. The rates of formation are not uniform and suggest that rates of formation can be locally higher. Previous workers suggested that dark slope streaks form with maximum contrast relative to adjacent surfaces, and then fade (brighten) with time as dust gradually accumulates. *Aharonson et al.* [2003] mentioned that all slope streaks present on Viking images are still present on MOC images and could not demonstrate any change in albedo. They thus argued that the formation and fading rate are not currently in balance. However, as emphasized by *Sullivan et al.* [2001], it is not possible to evaluate the possible slope streaks fading betweeen MOC and viking images. This would require the knowledge

of the atmospheric opacity at the time of acquisition and a photometric model taking into account the non-lambertian behavior for different conditions of illuminations. The rate of fading remains consequently an open question. *Sullivan et al.* [2001] observed few examples of new slope streaks formed systematically with a higher contrast showing that old slope streaks have faded. Given the present formation rates of slope streaks and the number of slope streaks, this observation suggests that slope streaks are currently fading. However, since the observation of a full erase of at least one slope streak is still missing, the fading rate and formation rate at the global scale appears not to be in balance. This persistence of streaks is intriguing but concerns only two and a half decades, while these rates could be perfectly in balance if integrated over hundreds or thousands of years.

3. Systematic mapping from HRSC data - methodology and results

3.1. Methodology

The main characteristics of the geometric properties can be described with three parameters, the length, the width and the apparent direction of the flow of the streaks (Fig. 3). The length is defined as the distance between the source point and the most distant point of the flow from the source. The width is defined as the maximum width of the streaks along the slope, and in a direction perpendicular to the apparent direction of the flow. The azimuth is defined as the apparent angle between the north and the direction of the flow given by the segment used for the length measurement. We never encountered any ambiguity in the definition of these parameters. The measurements have been achieved on orthorectified HRSC (High Resolution Stereo Camera) images. We use the global MOLA (Mars Orbital Laser Altimeter) DEM (Digital Elevation Model) at the 5 km grid-spacing for the orthorectification process. The images obtained correspond to the level 3 product

as defined in *Oberst et al.* [2004]. The length and orientation parameters are estimated for each slope streak from hand selected geographic coordinates of the source and edge of the slope streaks. The width is estimated from the hand selected geographic coordinates of the two points where the width of the streak reaches its maximum which is usually close to the end of the flow.

HRSC images from orbits 0024 and 0143 are used in this study, the maximum resolution at pericenter of nadir images of these orbits are 14 m and 16 m, respectively. Given that measurements are not made exactly at pericenter, we estimate errors for geometric measurements of about $20 - 30$ m, taking into account both pixel resolution and possible errors in the observation of the slope streaks boundaries. Slopes at the scale of streaks are not fully resolved by the DEM used in the orthorectification process, and an additional error of a few percent has to be considered. Some slope streaks have a curvature. In such a case, the length, measured from the source point to its end is underestimated by a few percent. These sources of error are significant for widths measurements, since a few percent of slope streaks have a width smaller than 20 m. For linear streaks, the error due to image resolution is negligible for length measurements. Errors in the orientation of slope streaks depend on errors in the localization of source and edge of the streaks. Given a typical length of 1 km and errors of 20 m, we estimate that orientations are given with an uncertainty of 2^o. For all these measurements over a given region, the frequencies of the lengths and widths are derived. The results of this systematic mapping are presented in the form of three contour maps obtained with a sliding window. The first represents the local slope streak density. The second represents the average orientation and the last gives the standard deviation of the average orientation within the sliding window. The

average value is considered to represent the value at the center of the sliding window. Slope streak density is equal to the number of slope streaks per unit area in the window. The average azimuth can be defined in two manners. It is first possible to estimate a mean slope streak vector $\vec{v}$ given by:

$$\vec{v} = \frac{1}{n}\sum_{i=1}^{n}(l_i \cos(\theta_i)\vec{x} + l_i \sin(\theta_i)\vec{y}) \tag{2}$$

where n is the number of slope streaks inside the window, l_i and θ_i are respectively the length and the azimuth of one given slope streak and $\vec{x}$ and $\vec{y}$ are the unit vector of the cartesian frame defined by the E-W and N-S axis. This definition implies that longer slope streaks will have more weight in the calculation. This definition has the advantage to assigning more weight to larger events recognizing that the amount of material involved in the process has to be taken in account in determining the factors of control of this phenomenon. However, if one considers that the lengths of slope streaks are mainly influenced by the lengths of slopes, this definition may reflect a bias toward the preferential orientation of longer slopes and it is possible to argue for another definition of the mean slope streak vector which is independent of the length of individual slope streaks:

$$\vec{v} = \frac{1}{n}\sum_{i=1}^{n}(\cos(\theta_i)\vec{x} + \sin(\theta_i)\vec{y}) \tag{3}$$

Both calculations have been made and do not display significant differences, indicating that the length distribution is independent of the flow direction. The results obtained with the first definition are presented. The standard deviation of the orientation represents the

width of the distribution of azimuths of the slope streaks inside the window and is given by:

$$\sigma = \frac{1}{n}\sqrt{\sum_{i=1}^{n}[\arccos(\frac{\vec{v_i} \bullet \vec{v}}{\|\vec{v_i}\|\|\vec{v}\|})]^2} = \frac{1}{n}\sqrt{\sum_{i=1}^{n}(\theta_i)^2} \quad (4)$$

where $\vec{v_i}$ is the vector defined by one given slope streak and $\|\vec{v}\|$ is the magnitude of the vector. This definition is a measure of the root mean square of the distances in angle unit (θ_i) between the vectors defined by individual slope streaks ($\vec{v_i}$) and the mean slope streak vector ($\vec{v}$).

The size of the window can influence the results. From different trials with different window sizes, the window size optimizing spatial resolution and statistical robustness has been selected. Values are presented using windows of 0.3^o of longitude by 0.3^o of latitude corresponding to 324 km^2 with a step of 600 meters between two successive centers of the sliding window.

3.2. Targets

We have focused on two regions having low thermal inertia, known for slope streak activity, and for which HRSC images were available. The first region extends from 10.2^oN to 12.0^oN and from 174.4^oE to 175.8^oE and corresponds to the border of Orcus Patera, in the vicinity of Cerberus lava flow. This terrain is of Noachian age. The relief could be attributed to eroded volcanic rocks and craters. The thermal inertia estimated from TES data [*Mellon et al.,* 2000, 2002] is relatively homogeneous and ranges from 30 $Jm^{-2}K^{-1}s^{-1/2}$ to 80 $Jm^{-2}K^{-1}s^{-1/2}$. The second region is a part of the Olympus Mons aureole and is named Lycus Sulci ridges. It extends from 28.0^oN to 38.0^oN and from

220.0^oE to 224.0^oE. Slope streaks are abundant in the aureole members units Aoa1, Aoa2, Aoa3 and Aoa4, as defined by *Tanaka and Scott* [1986]. These lobed units formed prior to or contemporaneously with the volcano's basal scarp and are more or less degraded, probably by aeolian activity. The average thermal inertia is about 30 $Jm^{-2}K^{-1}s^{-1/2}$ to 60 $Jm^{-2}K^{-1}s^{-1/2}$ with few localized areas at about 150 $Jm^{-2}K^{-1}s^{-1/2}$. The age of this surface is early Amazonian [*Tanaka and Scott,* 1986] and is thus recent compared to the first region. The high-frequency variations of thermal inertia suggest that the dust cover is heterogenous at local scale.

3.3. Geometric properties, widths, lengths and density

The geometric properties of slope streaks at Cerberus and at Licus Sulci ridges are similar. Lengths range from 200 meters to 1800 meters and the distribution is centered at 400 - 600 meters (Fig. 4). This value can be compared to the typical lengths ranging from 300 to 500 meters as found by Sullivan [2001] at the global scale. The maximum widths are more scattered ranging from few tens of meters to 250 meters (Fig. 5). These observations confirm the results obtained by Sullivan [2001]. The ratio between lengths and maximum widths ranges from 1.5 to 20 (Fig. 6). Sullivan [2001] observed exceptionally large ratios up to 50 but found a similar overall distribution. Gerstell et. al [2004] reported distributions of ratios for bright slope streaks and dark slope streaks respectively centered around 14.9 and 10.9 with similar standard deviations.

The uniformity of these geometric properties at the first order suggests that the same material and the same geological mechanism are involved in the formation of the slope streaks at the surface of Mars. The deposited dust in low-thermal inertia regions where slope streaks are observed results from long-term mixing at global scale of weathered rocks

and its composition and physical properties are expected to be homogeneous [*McSween and Kleil,* 2000; *Bell et al.,* 2000]. One may expect that the topography, the frequency of steep slopes, or the lengths of slopes may influence these geometric properties. In order to estimate this potential factor of control, the geometric properties are compared to roughness maps of the two regions. The roughness maps (Fig. 7) correspond to the root mean square elevation differences from an average tilted plane estimated locally with 5 kilometers diameter cells. This size was chosen considering the resolution of the MOLA DEM and the typical lengths of slope streaks. High values of roughness at this scale correspond to the presence of steep slopes at a wavelength of a few hundred meters. Relatively higher roughness values of 60 m to 100 m are more common at Licus Sulci ridges than at Cerberus. This difference may explain the slightly higher occurrence of long and large slope streaks at Olympus than at Cerberus. The exact slope at the source of the slope streaks may be a more relevant parameter to describe the influence of the topography but the resolution of available topographical data is currently not sufficient to address this issue. Finally, the surface roughness has a limited influence on the geometric properties of slope streaks. However, as described below, surface roughness is an essential factor of control of the occurrence of slope streaks.

The contour map of slope streak density (Fig. 9 and 11) reveals the heterogeneity of slope streaks distribution. This heterogeneity can be also directly observed on the map of slope streaks (Fig. 8 and 10). Densities ranging from 0 to 0.10 streaks/km^2 are observed. For the Olympus area, the average density between 29^oN and 33^oN is 0.013 ± 0.001 km^{-2} and is lower than the average density estimated by *Aharonson et al.* [2003] in the low thermal inertia regions (0.07 km^{-2}). However, we expect a possible bias from MOC

target selections, as mentioned by *Aharonson et al.* [2003]. Indeed, if areas containing steep slopes have been observed more frequently than flat areas, this would result in an artificially increased estimation. The slope streak density derived from the systematic mapping from HRSC is thus more robust. Taking the total area where slope streaks are observed equal to $2.3 * 10^7\ km^2$ as given roughly from the low thermal inertia regions [*Aharonson et al.,* 2003] and using our derived value as an average slope streak density over the whole planet, we find a total number of slope streaks of $300,000 \pm 20,000$. Slope streaks are rare, but not completely absent above 33^oN and are observed up to 37^oN, as indicated by the sparse observations in the same region [*Schörghofer et al.,* 2002]. *Schorghofer et al.* [2002] argued that slope streaks form only where surface temperature exceeds 275 K at least once a Martian year. For these high latitudes, the slope streak density is lower by one order of magnitude and this observation still suggests a potential role of H_20 at this point.

An ubiquitous correlation is observed with topography. The slope streak density maps are compared with roughness maps derived from the MOLA data (Fig. 7). For instance, at Olympus aureole, two regions of higher density, centered at 220.5^oE, 29^oN and 223^oE, 29.8^oN correspond to the highest roughness values of the area of about 200 meters. The slope streaks observed at the highest latitude are located in three areas, two craters centered at 222.1^oE, 34.7^oN and 221.8^oE, 35.5^oN and a narrow feature centered at 224.0^oE, 37^oN. These three areas correspond to roughness values greater than 100 m and are the roughest areas north of 34^oN inside the studied region. However, the correlation between the roughness and the slope streak density is not perfect. Two secondary peaks of slope streaks activity located at 220.5^oE, 30.4^oN and 221.2^oE, 31.5^oN do not correspond to

particular high roughness values. The correlation between roughness and density is also less clear at Cerberus area. These observations suggest that roughness is not the sole controlling factor.

3.4. Orientation

3.4.1. Cerberus.

Slope streaks at Cerberus are oriented preferentially on south to south-west facing slopes (cf. Fig. 12). West and East orientations are also possible but correspond to areas where the slope streak density is lower. A few slope streaks only occur on north facing slopes. This demonstrates that a preferential southward orientation does not occur exclusively above 30^oN but can also occur at lower latitude. This contradicts the expectations of *Schorghofer et al.* [2002] at the global scale. The relationship between the southward orientation and the potential role of H_20 given the conditions of illuminations at high latitude is thus questionable and other parameters, like wind directions may also influence the orientation of slope streaks.

3.4.2. Olympus Aureole.

Three distinct units can be distinguished from the map of average orientation (cf. Fig 13). The first unit corresponds to the few slope streaks observed at the highest latitudes. These northern slope streaks form essentially on south facing slopes. Average orientation is south to south-west and standard deviation is usually below 20^o, with only one region around 60^o.

The second unit is composed of the north-western part of the main zone of slope streaks activity (from about 30^oN to 33^oN and from 220^oE to 223^oE). These slope streaks form almost exclusively on south facing slopes, with progressively higher values for the standard

deviation toward the south-east (cf. Fig. 13), indicating that other orientations become possible. The preferential southward orientation is here consistent with what has been already observed at global scale for slope streaks occurring at latitudes higher than 30^o [*Schörghofer et al.,* 2002].

The third unit is composed of slope streaks forming preferentially on west facing slopes. The region extends from 29^oN to 31^oN and from 221.0^oE to 224.5^oE, with a higher range in latitude eastward. The standard deviation of the orientation is high, about 90^o revealing that other orientations remain possible. Indeed, this region is composed of two populations of slope streaks (Fig. 10), one population of slope streaks oriented almost exclusively on the west facing slope superposed to a second population of a smaller number of slope streaks oriented more randomly. If the rate of formation of slope streaks was dependent on the slope angle, the situation could be produced by steeper or more frequent west facing slopes than east facing slopes. An east-west topographic profile at 29.295^oN (Fig. 14) suggests that the occurrence and steepness of east facing slopes are similar to those of west facing slopes. We use 10 east-west topographic profiles between 219^oE and 225^oE covering the full range of latitudes of the area to estimate the distribution of slopes. The slopes were determined using three points derivative from the topographic profiles interpolated with a spacing of 1 km. The east facing slopes and west facing slopes have a similar range and a similar distribution (Fig. 15). The occurrence of slightly steeper slopes is not significant to explain our observations. Indeed, slope streaks are observed on projected slopes along the transect down to 10^o and the proportion of east and west facing slopes greater than 10^o is nearly identical (3.65% for east facing slopes and 3.79% for west facing slopes). It can be argued that slope asymmetry or steep scarps may be observed with a

higher resolution. This can not be investigated from MOLA data, but such an asymmetry would have been observed on MOC imagery at few meters resolution. We thus conclude here that the slope distribution can not be invoked at Licus Sulci ridges to explain the preferential formation of slope streaks on west facing slopes. In conclusion, preferential orientations of slope streaks have been observed at both sites. These orientations are not controlled by topography and an external factor is required. This suggests that the orientation of winds could be an essential factor of control. In order to investigate this hypothesis we will compare in the next section the wind directions with the preferential orientation of slope streaks.

3.5. Wind directions

The wind orientations pattern in the two studied regions can be investigated using a Global Circulation Model of the Martian atmosphere. The directions and intensity of winds as well as the quantity of dust transported in the Martian atmosphere are variable and depend on the season. The quantity of dust in the atmosphere may be estimated from the atmospheric opacity which has been observed throughout the MGS mission with the TES instrument. The peak of atmospheric opacity is detected near 255 degrees of solar longitude and corresponds to the season of maximum dust storm activity [*Smith et al.,* 2001]. It is observed that the dust storm season straddles Mars' perihelion which occurs at the beginning of the southern spring [*Smith et al.,* 2001; *Cantor et al.,* 2002]. The mechanism for dust-raising and dust storm abatement are poorly understood [*Smith et al.,* 2002]. It is generally proposed that the increased solar insolation coupled with the retreating south polar cap is responsible for the increase of winds speed which could be capable of lifting dust [*Smith et al.,* 2001]. Winds are thus stronger and the quantity of

dust in the Martian atmosphere is usually higher around the northern fall. The atmospheric circulation corresponding to this season has been computed at a high resolution of 2^o by 2^o using the Global Circulation Model developed at LMD and described in *Forget et al.* [1999] assuming the dust scenario as given by TES observations [*Smith et al.*, 2001]. Winds directions and intensity have been averaged over a period of 10 days centered at the solar longitude of 255^o and at 50 meters above the ground. Intensity and direction of winds are represented for Cerberus (Fig. 16) and Olympus Aureole (Fig. 17) areas. At Olympus, winds come from the east in the dusty season in the area where the population of slope streaks on west facing slopes have been observed. At Cerberus winds come from the north-east while the preferential orientation of slope streaks is south-west. The orientation of winds for the two regions are correlated with the preferential orientation of slope streaks. These results demonstrate that prevailing winds are a controlling factor of the slope streak formation.

3.6. Heterogeneities of the accumulation rate of dust

The preferential orientation on west facing slopes can be directly observed from MOC images (e.g., Fig. 18). The apparent paucity of craters on the west facing slopes relatively to other terrains, flat or steep, can be also noticed on these images. Dust sedimentation affects the morphology and regions covered by dust are characterized by smoothed topography at the MOC or HRSC resolution. In particular, the dust deposit can obliterate craters smaller than few tens of meters while larger ones remain visible. The depletion of small craters relative to larger ones has been occasionally used to estimate the local dust thickness and values of 7 to 19 meters have been obtained by *Vincendon et al.* [2002] for Arabia Terra. MOC images of the Licus Sulci ridges display variations of crater density

over distance of few hundreds of meters. Assuming that the ages of the ridges are similar, these variations which affect mainly the smallest craters represent heterogeneities of the dust thickness at the local scale. We thus interpret the paucity of craters on the west facing slope as an evidence of the higher net rate of dust accumulation which controls the formation of slope streaks.

We use one MOC image at Olympus Aureole where the slope streaks asymmetry was clearly observed with the objective to make a qualitative map of the dust thickness. All craters were counted, down to a diameter of a few pixels in order to estimate the local density of craters inside cells of 200 meters in diameter (Fig. 19). The distribution of crater sizes were not computed inside each cell, so absolute dust thickness is not estimated. However, variations in crater density represent relative variations in dust thickness. The number of craters per km^2 is represented by a color-coded map superposed over the MOC image. The resolution of the MOC image allows the observation of craters with diameters ranging from few tens of meters to few kilometers. Density up to 400 craters/km^2 are reported. The cumulative saturated crater density N_{cd} is given by [*Melosh,* 1989] :

$$N_{cd} = 1.54D^{-2} \tag{5}$$

From this equation, a surface having 400 craters/km^2 can be considered as saturated by impact if all craters were larger than 60 meters (about 10 pixels considering the resolution of 6.34 $m/pixel$ of the MOC image). Some craters smaller than 60 meters have been counted but given the uncertainty on the saturation estimation, it is reasonable to consider that the surface having 400 craters/km^2 is close to the equilibrium. Moreover, considering the isochrons of *Hartmann* [2005] and the saturation curve, the age of the

cratered surfaces are thus older than hundred millions years which is consistent with the Early Amazonian age indicated for this unit. Thus, the crater density variations do not reflect units of different ages but reveals that small craters have been buried by the dust cover. The obliterated craters can be both primary or secondary crater's ejecta. Areas in red correspond to the thinner dust cover. Areas with the thicker dust cover, corresponding to less than 10 craters per km^2, are not colored to outline the most dusty regions. All the slope streaks have been indicated with arrows. A strong correlation between the dustiest regions and the occurrence of slope streaks is observed. This correlation implies that slope streaks are dust avalanches controlled by the heterogeneities of dust deposition at the local scale. The wind direction is the primary factor of control of the dust deposition rate, as we will see in the next section dealing with snow avalanches on Earth as an analog explaining the occurrence and distribution of slope streaks.

4. Accumulation of wind transported dust control the occurrence of slope streaks

We have observed that wind orientations are highly correlated with the preferential orientation of slope streaks. The local rate of dust deposition implied by the observations of strong variations of dust thickness is also highly correlated with the slopes streaks activity. We thus propose that slope streaks are avalanches in dry granular material controlled by local heterogeneities in the accumulation rate of dust as hypothesized by Sullivan [2001]. These local variations are controlled by the wind orientations and the wind patterns around obstacles.

A very good analog of such a phenomenon is given by the heterogeneities of snow deposits controlled by wind directions and the triggering of avalanches at the downstream

side of the wind flow (Fig. 20). The wind pattern around obstacles is responsible for the formation of cornices and the accumulation of snow on the downstream side of the wind flow [*Michaux,* 2003; *Schweizer et al.,* 2003]. The accumulation of snow results from a decrease of the wind speed in the lee side of the crest. This phenomenon appears commonly in studies evaluating the risk of snow avalanches. The break of the cornice and the preferential accumulation of snow where the wind speed is reduced are responsible for the preferential triggering of avalanches on the lee slopes. Dust will also accumulate preferentially on the downstream side of the wind flow. The mechanical behaviour of a snow deposit may be more complicated than a dust deposit. For example, the phenomenon of melting and ice formation between snow flakes changing its cohesion does not operate in dry dust. The formation of dust cornices may therefore be limited. However, the wind pattern around obstacles will result in a preferential accumulation of dust in the downstream side of the wind flow, whatever the mechanical properties of dust are. In this case, the different rate of dust accumulation on slopes on the downstream side of the flow is responsible for avalanche occurrence. Dust avalanche may be triggered by an increase of the dust deposit due to the higher rate of accumulation.

5. Discussion

This study has demonstrated that slope streaks are avalanches of dust which are controlled by the local variations of dust sedimentation rate. In many places, as in Olympus or Cerberus, wind directions and wind pattern around obstacles may be responsible for these variations. As analogs, snow avalanches frequently result from higher accumulation rates of snow on slopes on the downstream side of the prevailing wind direction. However, the dynamics of dust avalanche differ from the dynamics of snow avalanche and is

discussed in more detailed below. The reason for the contrast change and the potential role of H_20 remains an issue beyond the scope of this study. The model of dust avalanche occurring in connection with higher rates of dust accumulation suggests that the contrast could be only due to the modification of the surface state of the dust layer. The possible contributions of both composition and surface state to the observed contrast are discussed below considering radiative transfer in granular material.

5.1. Dynamics of dust avalanches

Slope streaks seem to start and come to rest on a wide range of slopes, which is an intriguing observation given the dynamical properties of granular material are entirely defined by the critical angle and the angle of repose. In this section, we discuss the dynamics of dust avalanche, considered as a granular material. No definitive explanation of this observation can be provided here, since a complete analysis of the critical angle and angle of repose for slope streaks has not been achieved yet.

A pile of dry granular material with no cohesion does not flow until a certain angle is exceeded at the surface. This critical angle for the triggering of the avalanche depends on the grain properties and packing of the granular matter. The slope angle at which one slope streak starts is not yet resolved by available topographic data. Once the material is in motion, it stops at a lower angle, called the angle of repose. The angle of repose has been experimentally shown to depend on the shape and roughness of particles. The difference between the critical angle and the angle of repose may be due to the lower kinetic friction compared to static friction between the particles [*Samadani et al.,* 2001]. Repose angles ranging from 22^o for smooth particles, 33^o for Aeolian sands or 38^o for failed loess have been reported in *Lohnes and Handy* [1968]; *Carrigy* [1970]; *Hornbaker*

et al. [1997] and *Samadani* [2001]. The physical properties of soil deposits were measured during the Mars Pathfinder mission. Angles of repose measured with lander camera images average 34.2^o and are typically between 30^o and 38^o [*Moore et al.,* 1999]. Recent MER observations give however significantly higher values indicating the presence of cohesive soils throughout the upper 6 to 7 cm beneath the surface [*Ardvison et al.,* 2004a, 2004b]. Some recent experiments also focused on the angle of repose of Martian dust, and given the simulants material used, angle of repose ranging from around 30^o to 50^o have been found in *Möller* [2001]; *Möller et al.* [2002, 2003] and *Möller et al.* [2004]. It must be mentioned here that the size of the particles used in the simulant is larger by two orders of magnitude (75 μm) compared to the particle sizes of martian dust (< 2 μm) [*Clancy et al.,* 2003] . Given the distribution of slopes at Licus Sulci ridges, the slope angles on which slope streaks develop and come to rest appear to be generally lower than the expected angle of repose of a wide range of typical granular material.

The apparent diversity of slopes on which slope streaks occur and come to rest may be related to the diversity of particles shapes and sizes and may depend for instance on the proportion of dust and larger sand particles. A small amount of moisture or more probably frost that will increase the inter-particle cohesion could also change dramatically the angle of repose [*Samadani et al.,* 2001; *Hornbaker et al.,* 1997]. This presence of frost could be responsible for the diversity of slopes, for the stabilization of dust on north facing slopes around 30^oN and for the absence of slope streaks at higher latitude [*Schorghofer et al.,* 2002].

5.2. The contrast change: compositional or surface property effect ?

The reason for the contrast change is unresolved in this study. In the snow avalanche analog, the change of contrast in snow is due to a change of the surface roughness at the sub-pixel resolution as explained by *Helfenstein* [1988]. The change of roughness is due to clumping which is clearly seen when the avalanche is observed at a resolution of a few centimeters. The resulting contrast in that case corresponds to a modification of the photometric parameters and in particular of the shadowing function as defined in *Hapke* [1993]. Martian dust could have a similar behavior given its cohesion, its possible superficial induration and the presence of salt which may explain the formation of clumps. Streaks in snow appear darker or brighter depending of the conditions of illumination (Fig. 21), as predicted by the photometric models [e.g., *Hapke,* 1993]. An interesting example of streaks in snow displaying a contrast change has been observed and could be considered as an analog of slope streaks showing contrast changes on Mars (Fig. 22). On the left, the image of snow streaks shows a contrast change between the bright and smooth upper part and a rougher and darker deposit at the end of each streak. On the right, a martian slope streak displays a similar contrast change along the slope. This demonstrates that sliding of granular cohesive material can produce various changes in physical properties resulting in photometric parameters modifications. The surface texture, roughness and changes in grain size likely contribute to the contrast. To address this issue, photometric parameters inside the streaks and of the dust outside the streaks have to be determined. The photometric properties are particularly sensitive to the shapes of particles and a possible correlation between slope angles of streaks and photometric properties has to be investigated. We plan to use high-resolution DEM from HRSC/Mars Express

to achieve this analysis. The mechanism proposed above does not require a contribution of a change in the composition although it is not possible to rule out this hypothesis. A change in composition could be due to different degree of weathering of the dust exposed directly to the surface compared to the dust at few centimeters depth. Multi-angular observations from HRSC, using at least two or three different orbits combined with the high-resolution stereoscopic DEM are necessary to achieve the inverse modeling of photometric parameters, such as those appearing in the Hapke model, addressing both the contribution of surface texture and composition [*Pinet et al.,* 2005a, 2005b]. Large slope streaks observed in two or three different images with suitable conditions of observations are now being analyzed.

6. Conclusion

HRSC data have been used to map of the geometric characteristics and distributions of slopes streaks on two dusty regions known for their slope streaks activity. The main result of this mapping is the preferential orientations of slope streaks both at the highest latitudes and at the equator. These preferential orientations vary with the geographical location. We conclude that slope streaks are dust avalanches controlled by wind. Indeed, we have shown that (1) the preferential orientations of slope streaks are correlated with the wind directions estimated from a GCM at the season when the dust concentration in the atmosphere is the highest, (2) the density of slope streaks is correlated with the presence of a thicker dust cover, (3) the heterogeneity in the dust cover when a relief is present can be explained by the accumulation of dust in the downstream side of the wind flow, according to the computed wind direction. A potential role of H_2O in the triggering mechanism or flow can not be ruled out from this study, but all the characteristics of slope streaks

can be explained without invoking a phase transition of H_20 at the time of formation. Actually, the role of H_2O might be limited to a stabilizing effect on dust deposits on slopes at high latitudes as suggested in Schorghofer et al. [2002]. This would explain both the preferential orientation on south facing slopes at intermediate latitudes (30^oN - 33^oN) and the paucity of slope streaks at relatively higher latitudes. Snow avalanches are proposed as good analogs of these dust avalanches on Mars. The comparison of these features suggests that a change in the physical surface state (roughness, grain size) instead of a change in albedo may be the major contribution to the contrast change. This hypothesis has to be investigated further using multi-angular HRSC data in order to estimate photometric parameters of the dust deposits and inside the slope streaks. HRSC data set, given the increasing coverage at high resolution and areas observed with time intervals of several months to about one year, will be also used to confirm the present rate of formation of slope streaks and address the issue concerning the balance with the rate of fading.

Acknowledgments.

This project has been supported by the Programme National de Planétologie and by the CNES (French Spatial Agency). N. Schorghofer and an anonymous review provided helpful reviews and their suggestions improved the clarity of the manuscript. V. Kaydash made thoughtful suggestions concerning the photometric behavior of granular material.

References

Aharonson, O., Schorghofer, N., Gerstell, M., 2003. Slope streaks formation and dust deposition rates on Mars. Journal of Geophysical Research 108(E12), 5138, doi: 10.129/2003JE2003JE002123.

Arvidson, R. E., 29 colleagues, 2004. Localization and physical properties experiments conducted by Spirit at Gusev crater. Science 305, 821–824, doi:10.1126/science.1099922.

Arvidson, R.E., 23 colleagues, 2004. Localization and physical property experiments conducted by Opportunity at Meridiani Planum. Science 306, 1730-1733, doi: 10.1126/science.1104211.

Bell III, J.F., 23 colleagues, 2000. Mineralogic and compositional properties of Martian soil and dust: results from Mars Pathfinder. Journal of Geophysical Research, 105(E1), 1721–1755.

Cantor, B., James, P., Caplinger, M., Wolff, M., 2001. Martian dust storms: 1999 mars orbiter camera observations. Journal of Geophysical Research 106(E10), 23653–23687.

Clancy, R.T., Wolff, M.J., Christensen, P.R., 2003. Mars aerosols studies with the MGS TES emmission phase funcion observations: Optical depths, particle sizes, and ice cloud types versus latitude and solar longitude. Journal of Geophysical Research 108(E9), 5098, doi:10.129/2003JE002058.

Carrigy, M. (1970). Experiments on the angles of repose of granular material. Sedimentology 14, 147–158.

Ferguson, H. M., Lucchitta, B.K., 1984. Dark streaks on talus slopes, Mars, in Planetary Geology and Geophysics Program Report, pp. 188-190.

Ferris, J., Dohm, J., Baker,V. R. and Maddock, R., 2002. Dark slope streaks on Mars: Are aqueous processes involved ? Geophysical Research Letters 29(10), 128–1,128–3.

Forget, F., Hourdin, F., Fournier, R., Hourdin, C., Talagrand, O., Collins, M., Lewis, S., Read, P., Huot, J.P., 1999. Improved general circulation models of the martian atmosphere from the surface to above 80 km. Journal of Geophysical Research 104(E10),

24155–24176.

Gerstell, M.F., Aharonson, O., Schoghofer, N., 2005. A distinct class of avalanche scares on Mars. Icarus 168, 122-130.

Hapke, B., 1993. Theory of reflectance and emittance spectroscopy. Topics in remote sensing 3. Cambridge University Press.

Hartmann, W. K., 2005. Martian cratering 8: Isochron refinement and the chronology of Mars. Icarus 174, 294–320.

Helfenstein, P., 1988. The geological interpretation of photometric surface roughness. Icarus 73, 462–481.

Hornbaker, D., Albert, R., Albert, A.-L., Barabási, I., Schiffer, P., 1997. What keeps sandcastles standing. Nature 387, 765.

Lohnes, R., Handy, R., 1968. Slope angles in friable loess. Journal of Geology 76(3), 247–258.

Malin, M. C., Edgett, K., 2001. Mars Global Surveyor Mars Orbiter Camera: Interplanetery cruise through primary mission. Journal of Geophysical Research 106(E10), 23429–23570.

McSween, H. Y., and Keil, K., 2000. Mixing relationships in the Martian regolith and the composition of globally homogeneous dust. Geochemica et Cosmochimica Acta 64(12), 2155–2166.

Mellon, M. T., Jakosky, B., Kieffer, B.M., Christensen, P.R., 2000. High-resolution thermal inertia mapping from the Mars Global Surveyor Thermal Emission Spectrometer. Journal of Geophysical Research 148, 437–455.

Mellon, M. T., Kretke, K. A., Smith, M. D., Pelkey, S.M., 2002. A global map of thermal inertia from Mars Global Surveyor mapping mission. XXXIII Lunar and Planetary Science Conference, Houston, abstract #1416.

Melosh, H.J., 1989. Impact cratering, a Geologic Process, Oxford monographs on geology and geophysics No11. Oxford University Press. Clarendon University Press.

Michaux, J.-L., 2003. Etude, compréhension, et modélisation des phénomènes liés au transport de la neige par le vent, PhD thesis, Université Joseph Fourier, Grenoble.

Miyamoto, H., Dohm, J., Beyer, R., Baker, V., 2004. Fluid dynamical implications of anastomosing slope streaks on mars. Journal of Geophysical Research 109(E06008), doi:10.129/2003JE002234.

Möller, L., 2001. Critical angle of repose of martian dust. XXXII Lunar and Planetary Science Conference, Houston, abstract #1470.

Möller, L., Kuhlman, K. , Marshall, J. Towner, M., 2002. The snooy angle experiment: calibration of an instrument to determine the angle of repose of martian dust. XXXIII Lunar and Planetary Science Conference, Houston, abstract #2015.

Möller, L., Tuller, M., Baker, L., Marshall, J., Castiglione, P., Kuhlman, K., 2003. Experimental study of the angle of repose of surrogate martian dust. Lunar and Planetary Science Conference, Houston, abstract #1526.

Möller, L., Tuller, M., Islam, M., Baker, L., Kuhlman, K., 2004. Mars environment chamber for dynamic dust deposition and statics analysis. XXXV Lunar and Planetary Science Conference, Houston, abstract #1773.

Moore, H.J., Bickler, D.B., Crisp, J.A., Howard, J.E., Gensler, J.A., Hadelman, A.F.C., Matijevic, J.R., Ried, L.K., 1999. Soil-like deposit observed by Sojourner, the Pathfinder

rover. Journal of Geophysical Research 104(E4), 8729–8746.

Morris, E., 1982. Aureole deposits of the Martian volcano Olympus Mons. Journal of Geophysical Research 87, 1164–1178.

Motazedian, T., 2003. Currently flowing water on Mars. XXXIV Lunar and Planetary Science Conference, Houston, abstract #1840.

Oberst, J., 15 colleagues 2004, The mapping performance of the HRSC / SRC in Mars orbit. ISPRS. vol. Commission IV, Istanbul.

Pinet, P., Cord, A., Jehl, A., Daydou, Y., Chevrel, S., Baratoux, D., Greeley, R., Williams, D. Neukum, G., HRSC Co-Investigator Team, 2005. Mars express imaging photometry and surface geologic processes at mars: What can be monitored within gusev crater ? XXXVI Lunar and Planetary Science Conference, Houston, abstract #1721.

Pinet, P., 16 colleagues, 2005. Orbital imaging photometry and surface geologic processes within gusev. European Geophysical Union, Vienna, vol. 7, abstract #09363.

Pinet, P.,16 colleagues, 2005c, Derivation of mars surface scattering properties from omega spot pointing observations. XXXVI Lunar and Planetary Science Conference, Houston, abstract #1694.

Samadani, A., Kudrolli, A., 2001. Angle of repose and segregation in cohesive granular matter. Physical Review E64(05301), 1–9, doi:10.1103/PhysRevE.64.051301.

Schorghofer, N., Aharonson, O., Khatiwala, S., 2002. Slope streaks on mars: Correlations with surface properties and the potential role of water, Geophysical Research Letters 29(23), 2126, doi:10.1029/2002GL015889.

Schweizer, J., Jamieson, J.B., Schneebeli, M., 2003. Snow avalanche formation. Reviews of Geophysics 41(4), 1016, doi:10.1029/2002RG00123.

Seelos, F., Arvidson, R., Guiness, E., Wolf, M., Athena Science Team, 2005. Radiative transfer photometric analyses at the Mars Exploration Rover landing sites. XXXVI Lunar and Planetary Science Conference, Houston.

Smith, M.,Pearl, J. C., Conrath, B., Christensen, P.R., 2001. Thermal emission spectrometer results: Mars atmospheric thermal structure and aerosol distribution. Journal of Geophysical Research 106(E10), 23929–23945.

Smith, M., Conrath, B., Pearl, J.C., Christensen, P.R., 2002. Thermal emission spectrometer observations of martian planet-encircling dust storm 2001a. Icarus 157, 259–263, doi:10.1006/icar.2001.6797.

Sullivan, R., Thomas, P., Veverka, J., Malin, M., Edgett, K., 2001. Mass movement slope streaks imaged by the Mars Orbiter Camera. Journal of Geophysical Research 106(E10), 23,607–23,633.

Tanaka, K., Scott, D., 1986. Geologic map of the western equatorial region of Mars.

Vincendon, C., Mangold, N., Masson, P., Ansan, V., 2002. Estimation of dust thickness in arabia terra region. XXXIII Lunar and Planetary Science Conference, Houston, abstract #1208.

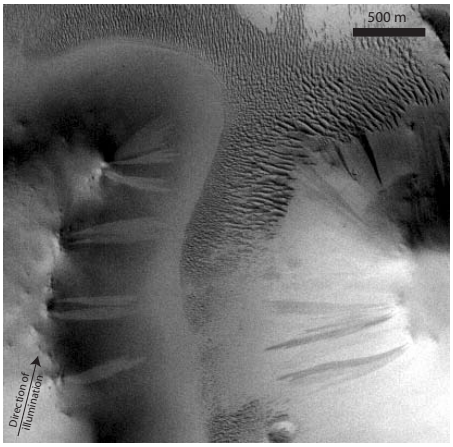

Figure 1. MOC image E1001445 showing bright and dark slope streaks on opposite slopes suggesting that the contrast of slope streaks depends on the conditions of illumination.

Figure 2. MOC image R1104122 in Arabia Terra showing bright and dark slope streaks intermingled on the same slope. This observation is not consistent with the hypothesis that the contrast of the streaks depends on the conditions of illumination assuming that the streaks are always associated with a similar change in the photometric parameters.

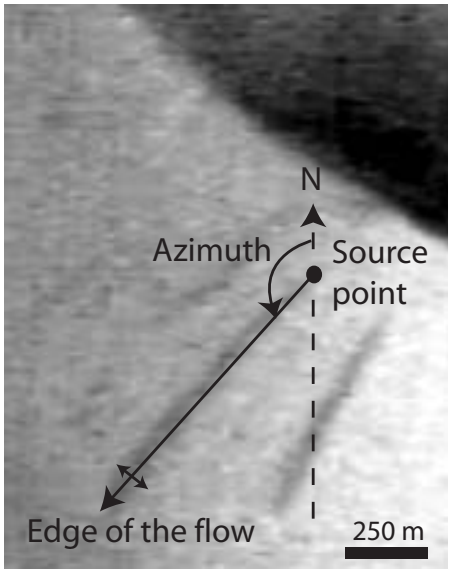

Figure 3. Measurement of length, width and azimuth of slope streaks on level 3 HRSC images.

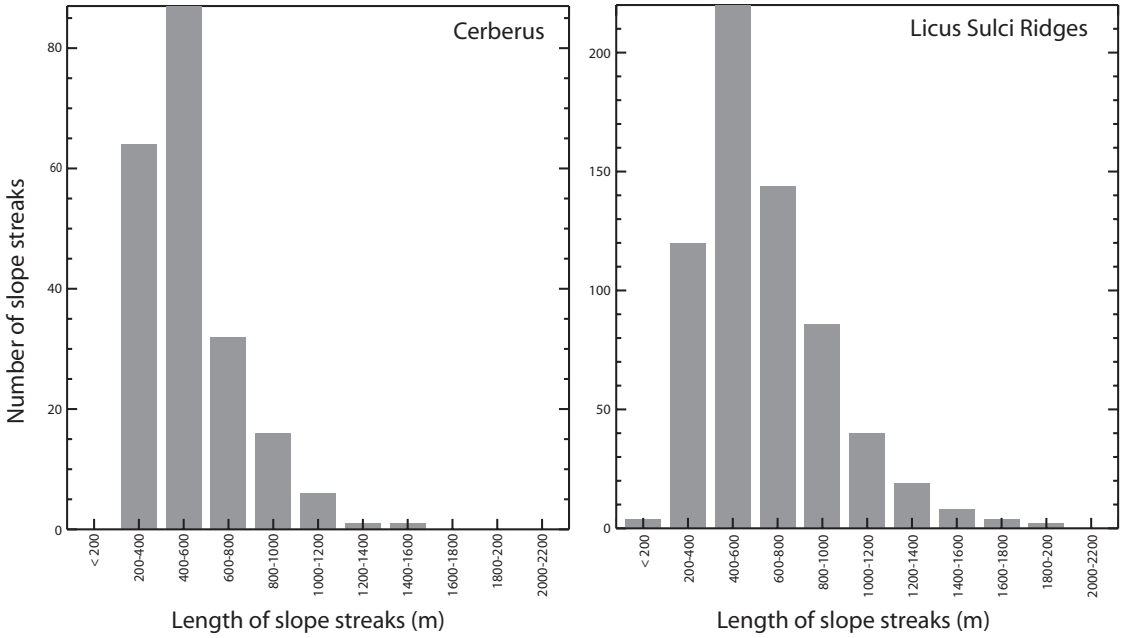

Figure 4. Histograms of slope streaks lengths for Cerberus and Olympus Aureole.

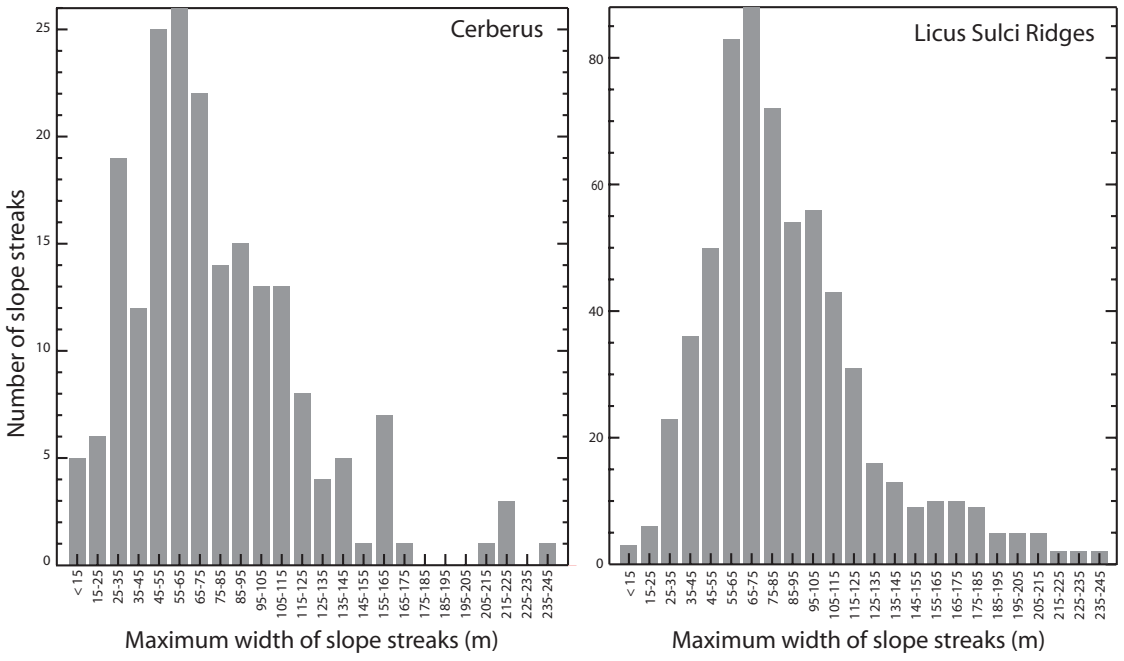

Figure 5. Histograms of slope streaks widths for Cerberus and Olympus Aureole.

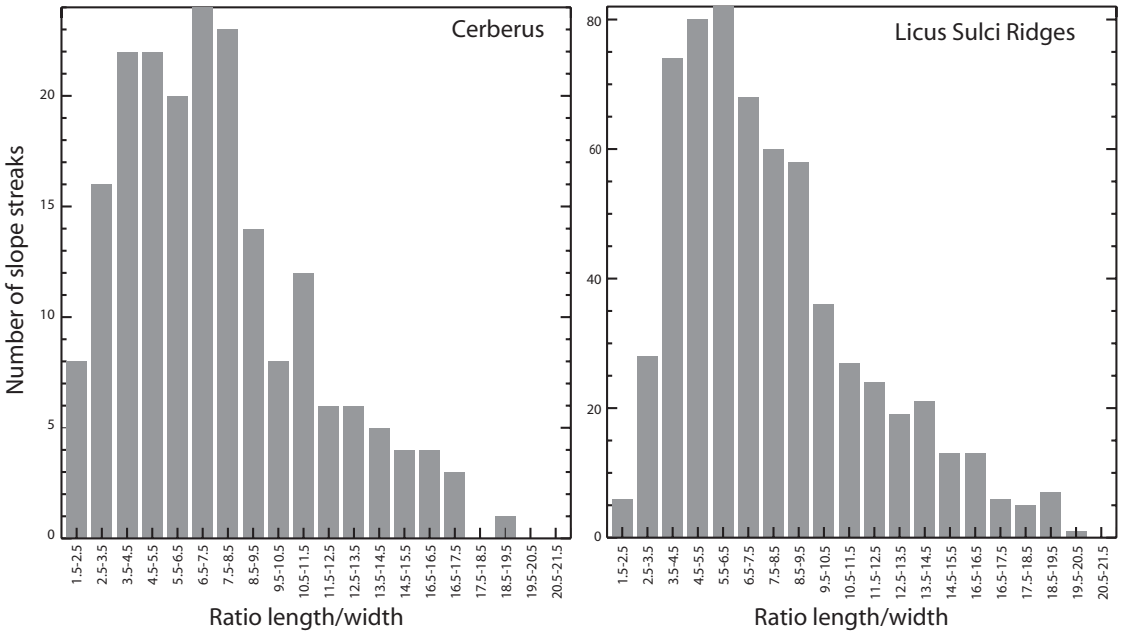

Figure 6. Histograms of slope streaks ratios lengths/widths for Cerberus and Olympus Aureole.

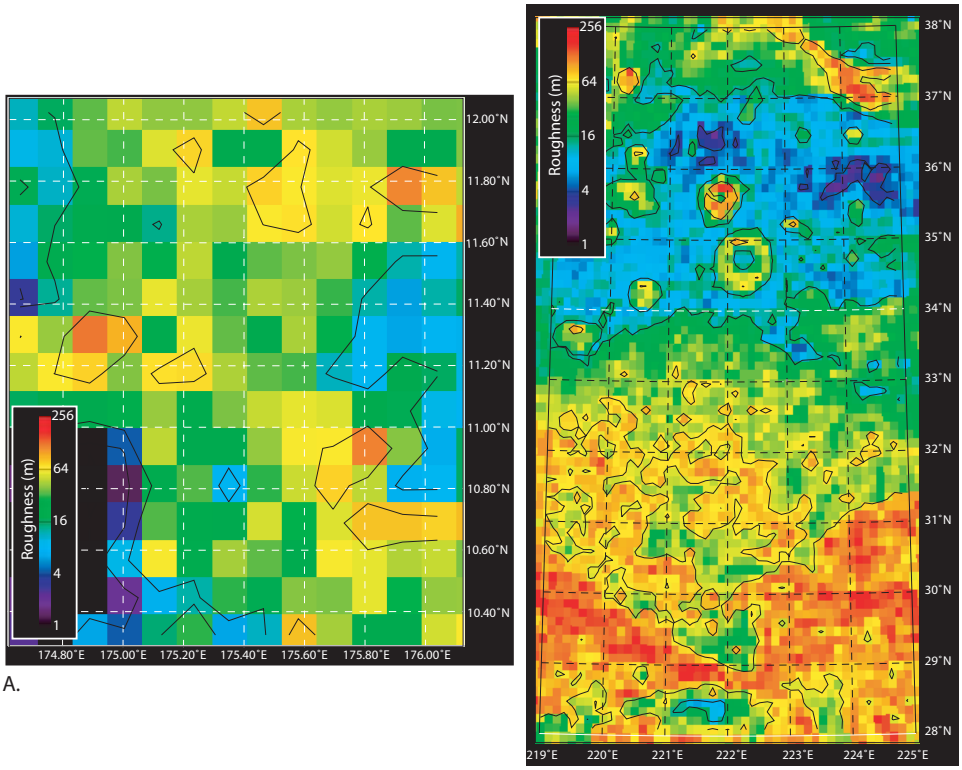

Figure 7. A. Roughness map from the MOLA data at Cerberus. B. Roughness map from MOLA data at Olympus. The roughness is computed as the standard deviation of elevations from an average plane given the elevations inside a cell of 5 km in diameter. Isoroughness lines are plotted for 1, 4, 16, 64 and 256 m.

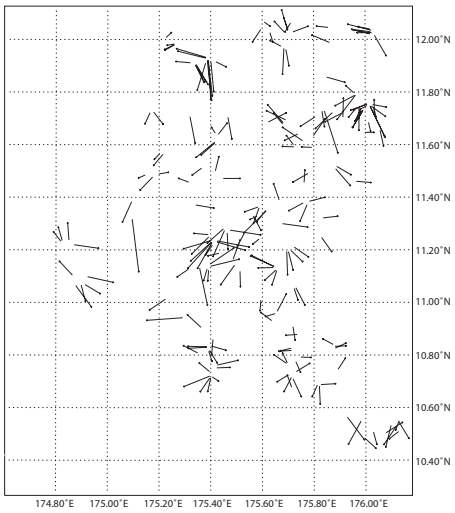

Figure 8. Map of slope streaks at Cerberus. The size of the arrows represents 8 times the length of the slope streak.

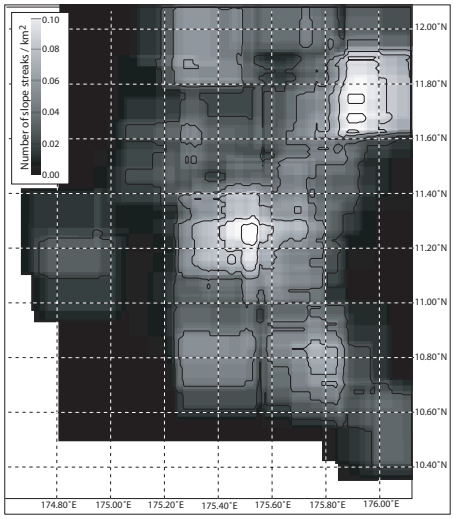

Figure 9. Slope streak density at Cerberus estimated using a sliding window of 0.3^o of longitude by 0.3^o of latitude. Isodensity lines are plotted for density of 0.0, 0.02, 0.04, 0.06, 0.08 and 0.10 streaks/km^2.

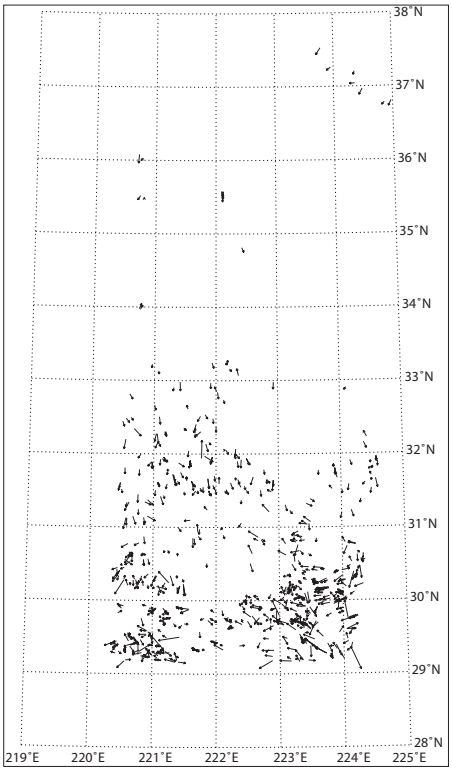

Figure 10. Map of slope streaks at Olympus. The size of the arrows represents 8 times the length of the slope streak.

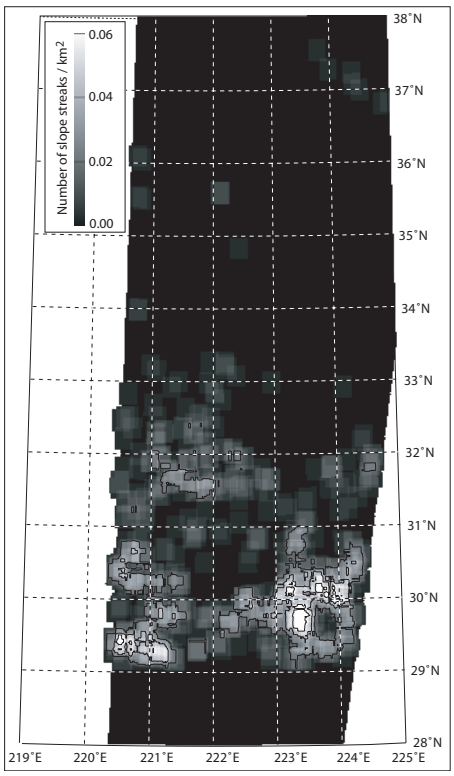

Figure 11. Slope streak density at Olympus Aureole estimated using a sliding window of 0.3^o of longitude by 0.3^o of latitude. Isodensity lines are plotted for density of 0.0, 0.02, 0.04 and 0.06 streaks/km^2.

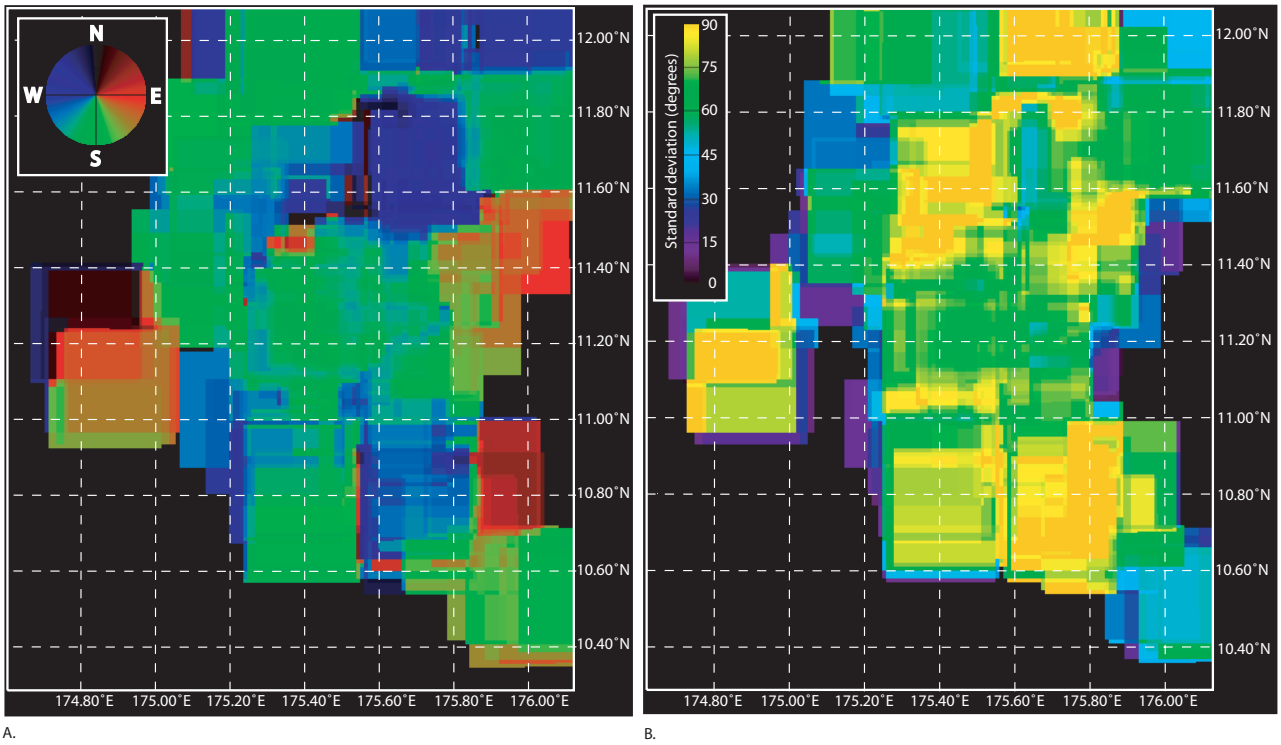

Figure 12. A. Map of the mean orientation of slope streaks at Cerberus. B. Map of the standard deviation of the mean orientation at Cerberus. The slope streaks orientation and standard deviation are estimated within the 0.3^o*0.3^o rectangular cells.

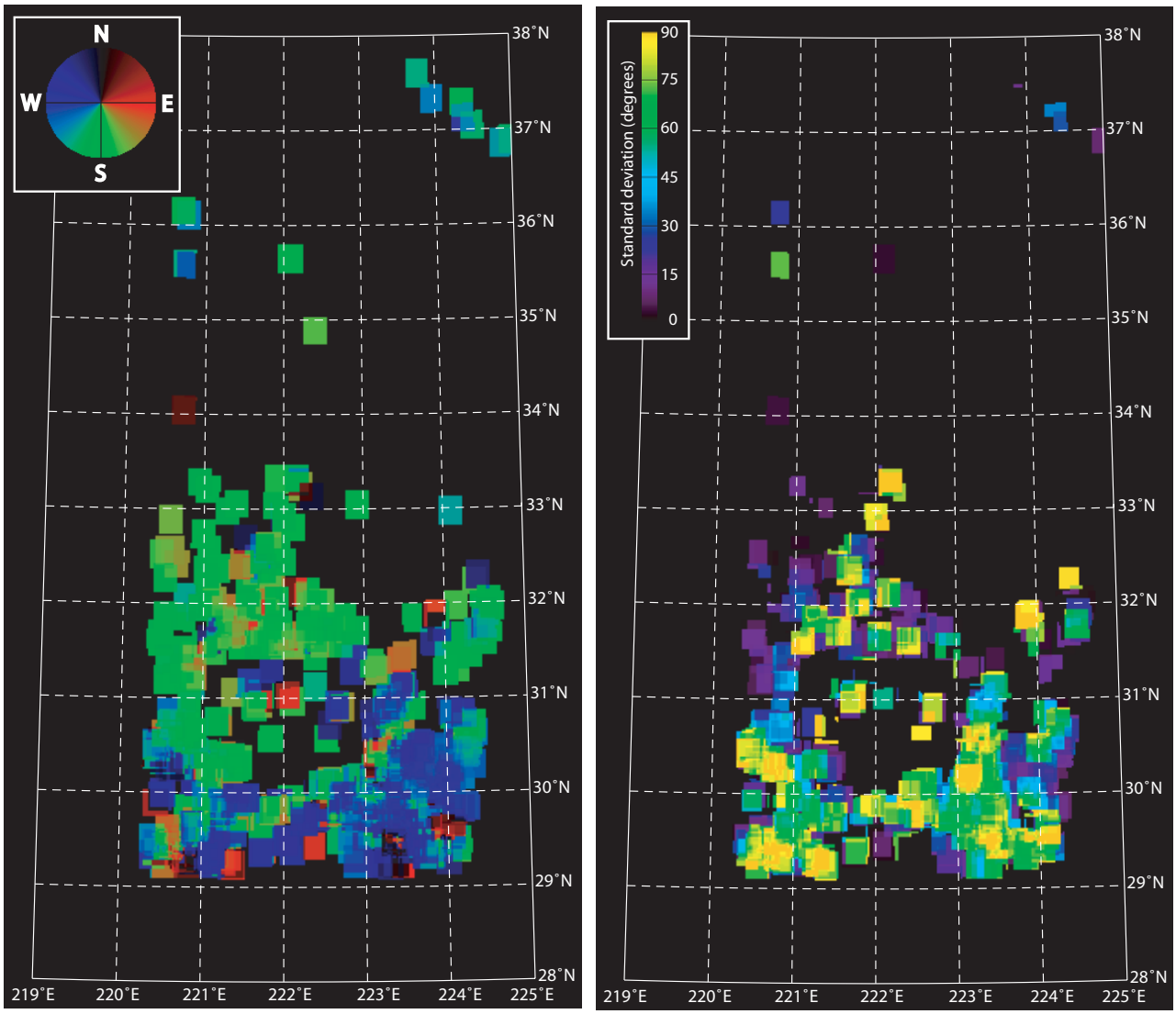

Figure 13. A. Map of the mean orientation of slope streaks at Olympus. B. Map of the standard deviation of the mean orientation at Olympus. The slope streaks orientation and standard deviation is estimated within the 0.3^o*0.3^o rectangular cells.

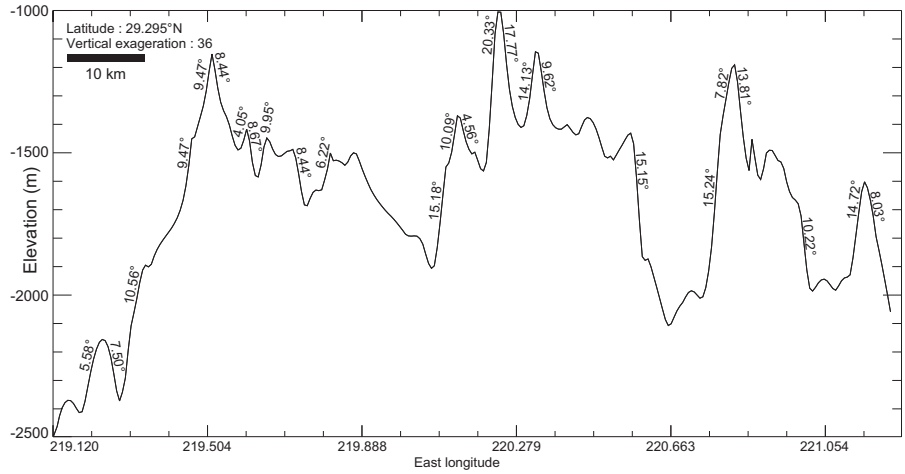

Figure 14. Example of an east-west topographic profile at Licus Sulci ridges. Slopes have been estimated using 1 km segments. No east/west asymmetry can be demonstrated from this example.

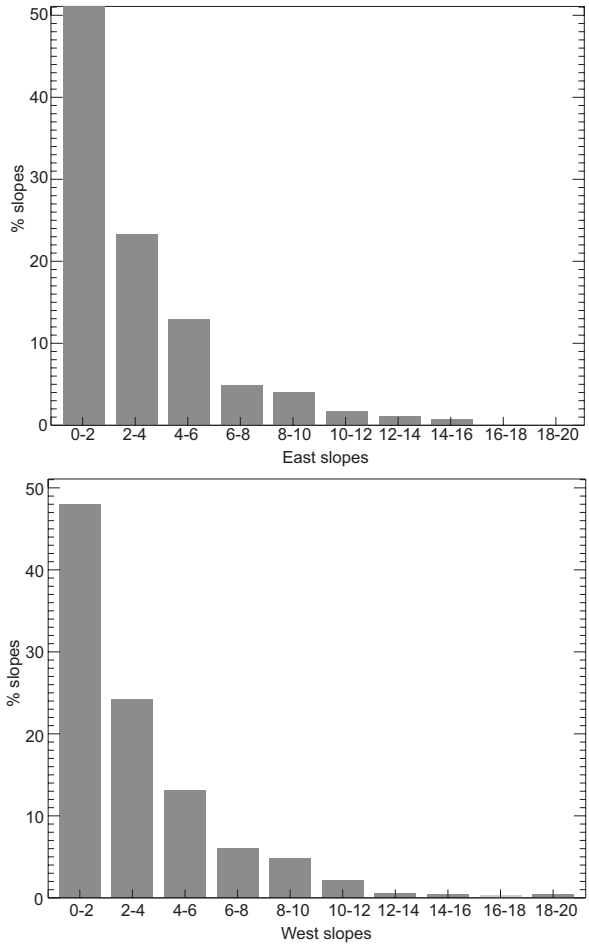

Figure 15. Distribution of east and west facing slopes at Licus Sulci ridges from 219^oE and 223^oE from 10 east-west topographic profiles between 28^oN and 31.60^oN. The slopes were determined using three points derivative from the topographic profiles interpolated with a spacing of 1 km.

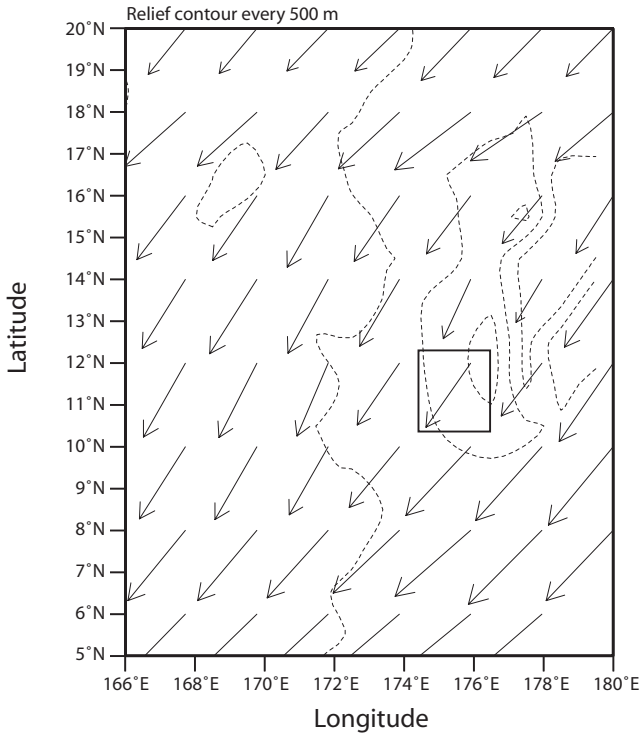

Figure 16. Wind direction simulated with a high resolution of 2^o by 2^o at 50 meters elevation in the dusty season at Cerberus. The square represents the mapped region.

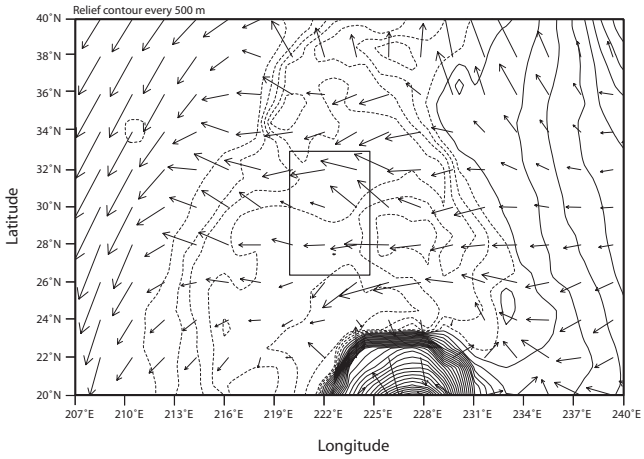

Figure 17. Wind direction simulated with a high resolution of 2^o by 2^o at 50 meters elevation in the dusty season (10 days averaged around 255^o of solar longitude) at Olympus aureole. The square represents the mapped region.

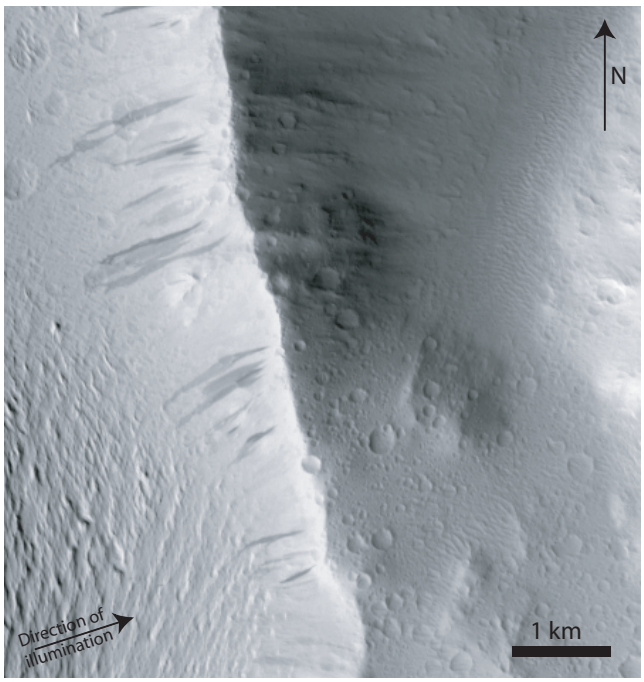

Figure 18. Example of a MOC image over Licus Sulci ridges showing a west facing slope with numerous slope streaks associated with a depletion of small craters and the presence of large subdued craters. Conversely, the east facing slope displays small craters. This image strongly suggests a dependence between the local dust thickness and the presence of slope streaks.

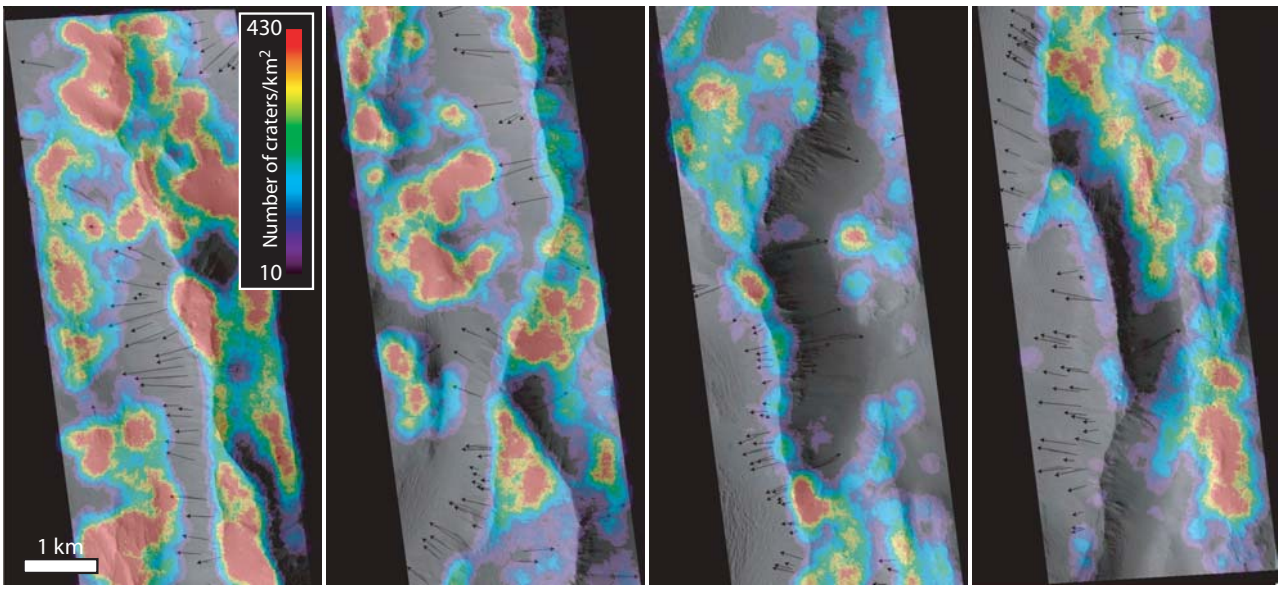

Figure 19. Local density of craters (number of craters / km^2) superposed over the MOC image $R0301511$. Arrows outline the slope streaks. Areas in red indicate a thinner dust cover. No color is displayed for values lower than 10 craters / km^2 so these most dusty regions can be seen in transparence. Note the strong correlation between the dustiest regions and the occurrence of slope streaks.

Figure 20. Example of slope streaks analogs in snow. The wind came from the back of the picture and is responsible for the formation of the cornices. The accumulation of snow at the crest and along the slope produces three snow avalanches on the downstream side of the wind flow.

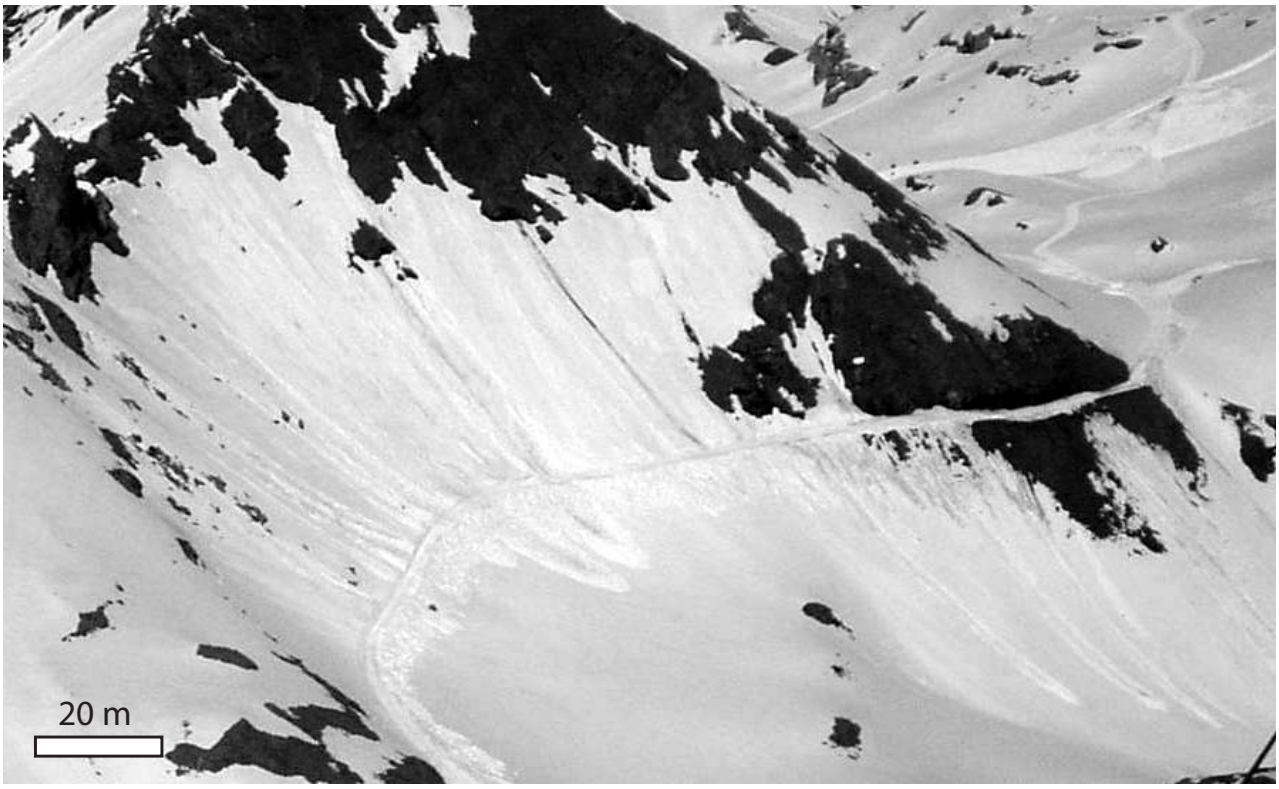

Figure 21. Streaks in the snow appear brighter at lower phase angle. This example illustrates how the conditions of illuminations and observations can influence the contrast of granular material on adjacent terrains.

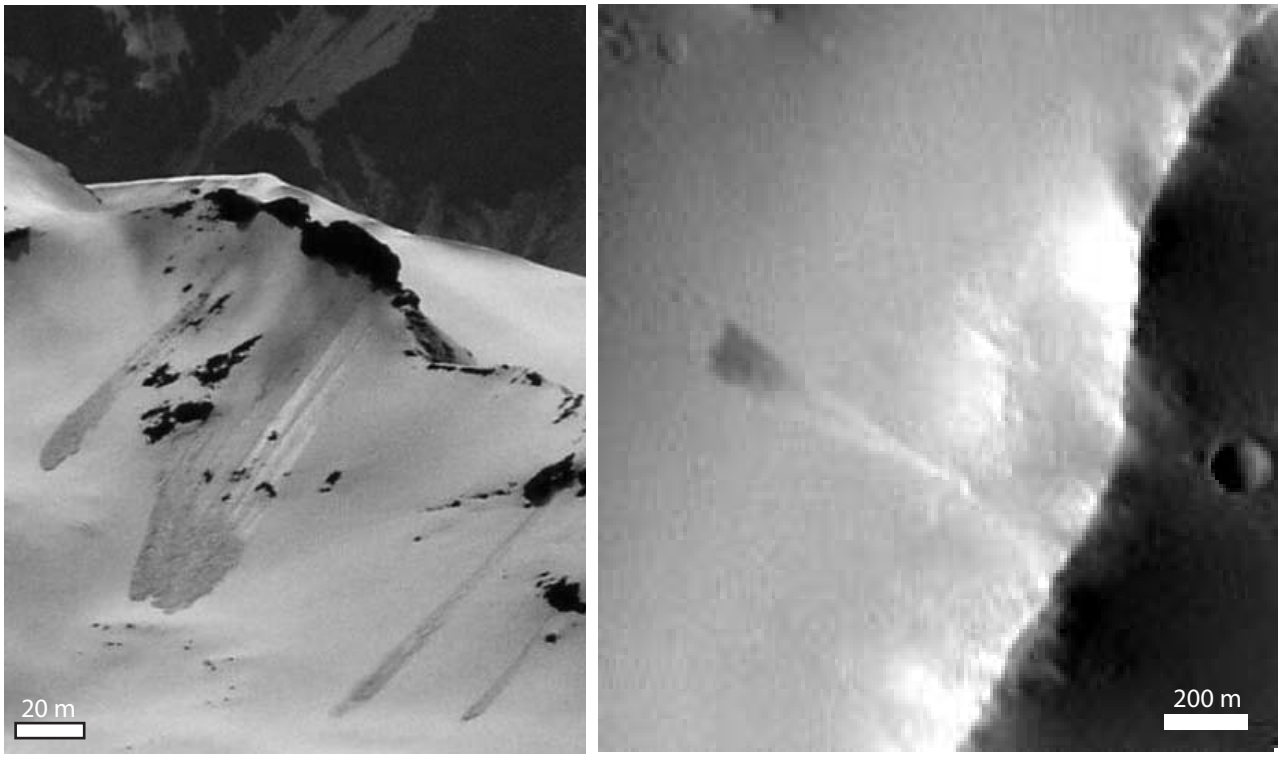

Figure 22. Example of a contrast change in snow avalanche along the slope and its counterpart on Mars. This example illustrates the possible changes in photometric properties along the slope and could also explain the observation of both brighter and darker streaks on the same slopes.